



## Article

# An Ultra-Sensitive Colorimetric Sensing Platform for Simultaneous Detection of Moxifloxacin/Ciprofloxacin and Cr(III) Ions Based on Ammonium Thioglycolate Functionalized Gold Nanoparticles

Lihua Zhang <sup>1</sup>, Jiang Li <sup>1</sup> , Juan Wang <sup>1</sup>, Xu Yan <sup>1</sup>, Jinping Song <sup>2</sup> and Feng Feng <sup>1,\*</sup> 

<sup>1</sup> Shanxi Provincial Key Laboratory of Chemical Biosensing, School of Chemistry and Chemical Engineering, Shanxi Datong University, Datong 037009, China; lihuazhang888@163.com (L.Z.); possumlee@126.com (J.L.); juanwang0422@163.com (J.W.); xuyan04032025@163.com (X.Y.)

<sup>2</sup> Department of Chemistry, Xinzhou Normal University, Xinzhou 034000, China; songjphx@163.com

\* Correspondence: feng-feng64@263.net

## Highlights

### What is the main findings?

- ATG-functionalized AuNPs were prepared as a colorimetric chemosensor with ultra-sensitivity for the simultaneous detection of MOX/CIP and Cr(III).

### What are the implications of the main findings?

- ATG-AuNPs sensor color transitions from wine-red to gray-blue indicated successful detection.
- The detection limits for MOX/CIP and Cr(III) are 1.57  $\mu\text{M}$ , 1.30  $\mu\text{M}$ , and 57.1 nM, respectively.
- The presented method was used to detect multiple analytes in lake and tap water samples.



Academic Editor: Debanjana Ghosh

Received: 16 April 2025

Revised: 13 May 2025

Accepted: 15 May 2025

Published: 21 May 2025

**Citation:** Zhang, L.; Li, J.; Wang, J.; Yan, X.; Song, J.; Feng, F. An Ultra-Sensitive Colorimetric Sensing Platform for Simultaneous Detection of Moxifloxacin/Ciprofloxacin and Cr(III) Ions Based on Ammonium Thioglycolate Functionalized Gold Nanoparticles. *Sensors* **2025**, *25*, 3228. <https://doi.org/10.3390/s25103228>

**Copyright:** © 2025 by the authors. Licensee MDPI, Basel, Switzerland. This article is an open access article distributed under the terms and conditions of the Creative Commons Attribution (CC BY) license (<https://creativecommons.org/licenses/by/4.0/>).

**Abstract:** Water pollution by antibiotics and heavy metals threatens the ecological environment and human health globally, yet there is no rapid method to detect multiple antibiotics and metal ions simultaneously. A simple, fast, and ultra-sensitive colorimetric chemosensor for the simultaneous detection of moxifloxacin (MOX), ciprofloxacin (CIP), and Cr(III) based on the aggregation of ammonium thioglycolate (ATG)-functionalized gold nanoparticles (ATG-AuNPs) was developed. Following the addition of MOX, CIP, and Cr(III), a color change in the solution was observed from wine-red to blue-grey. The UV–Vis signal of the ATG-AuNPs system blended with MOX, CIP, and Cr(III) in the range of 0~200  $\mu\text{M}$ , 0~100  $\mu\text{M}$ , and 0~5  $\mu\text{M}$  was assessed and measured with detection limits (LODs) of 1.57  $\mu\text{M}$ , 1.30  $\mu\text{M}$ , and 57.1 nM calculated by  $3\sigma/S$ , respectively. Therefore, this system has the potential to act as an effective colorimetric chemosensor for simultaneously detecting MOX, CIP, and Cr(III) in complex environmental systems.

**Keywords:** colorimetric chemosensor; ammonium thioglycolate; moxifloxacin (MOX); ciprofloxacin (CIP); Cr(III); gold nanoparticles

## 1. Introduction

Antibiotics and heavy metal pollution pose significant risks to public health and the environment worldwide. Moxifloxacin (MOX) and ciprofloxacin (CIP) are popular

broad-spectrum quinolone antibiotics exhibiting high activity against various bacterial species, both Gram-negative and Gram-positive [1,2]. They have been employed in treating severe-to-moderate community intravenous pneumonia, infections of the skin and soft tissues, acute sinusitis with bacteria caused by susceptible microorganisms, and acute bacterial chronic bronchitis [3]. They have also been used for diseases caused by bacteria resistant to other antibiotics, such as aminoglycosides and  $\beta$ -lactams [4]. As a result, large amounts of residues of MOX and CIP are inevitably discharged into the surrounding environment and food, subsequently accumulating in the human body via the biological cycle; uncontrolled utilization of MOX and CIP may induce human diseases and result in their excretion in an unchanged form through urine, leading to considerable detrimental effects on human health and environmental issues [5,6]. Organizations and countries have established maximum residue limits (MRLs) to reduce the misuse of antibiotics in various food products. For instance, India has set a maximum residue limit of  $1.0 \mu\text{g}/\text{kg}$  for MOX in food samples. Moreover, the European Union has established a maximum residue limit (MRL) for certain fluoroquinolones, including CIP, in edible animal products, set at  $30 \mu\text{g}\cdot\text{kg}^{-1}$  for various edible animal tissues [7]. In addition, the trivalent chromium ion (Cr(III)) is another molecule that poses a health risk to humans, being one of the most prevalent heavy metal ions in industrial effluent, and has the potential for accumulation in the human body through the food chain [8,9]. Although Cr(III) is a vital micronutrient that can efficiently sustain the metabolic functions of carbohydrates, adipose tissues, and proteins in the human body [10], an excessive intake of Cr(III) can bind robustly to DNA in human cells, negatively changing their cellular structure and composition and thereby elevating the risks of DNA damage and cancer [11]. Considering the complexity of sample detection environments, as mentioned above, there is an urgent need to develop a new simultaneous detection method that possesses the advantages of being simple, cheap, and having high sensitivity for simultaneous identification and distinguishing between MOXI/CIP and Cr(III) by a standalone system.

Up until now, a variety of plentiful approaches have been developed to detect MOX/CIP or metal ions, such as high-performance liquid chromatography (HPLC) [12–14], liquid chromatography–mass spectroscopy (LC-MS) [15–17], gas chromatography–mass spectroscopy (GC-MS) [18], inductively coupled plasma–mass spectrometry (ICP-MS) [19,20], electrochemical methods [21–23], gas atomic absorption spectrometry (AAS) [24,25], and fluorescence detection [26–28]. However, these approaches are costly, time-consuming, and laborious and demand sophisticated analysis procedures, restricting their use in the field. Consequently, developing a simultaneous detection system that is straightforward, rapid, inexpensive, and yet offers enhanced performance is essential.

Among the detection techniques, colorimetric sensors have attracted considerable attention since they facilitate simple, rapid, and real-time measurement without sophisticated apparatus [29]. Gold nanoparticles (AuNPs) are frequently employed as colorimetric reporters due to their distance-dependent optical properties [30]. The extinction spectra of AuNPs and their absorbed and dispersed light wavelength depend on the interparticle distance [31]. Therefore, systems based on the analyte-driven aggregation of AuNPs have been utilized for the colorimetric sensing of specific analytes through detection reporters on the AuNPs [32–39]. Notably, the ability of a single sensor to simultaneously detect multiple analytes has recently gained significant attention, owing to advantages including cost reduction and improved analytical efficiency [40–44]. Consequently, the design and synthesis of colorimetric sensors exhibiting high selectivity and sensitivity toward MOX, CIP, and Cr(III) have attracted increasing attention [45–47]. Recent advances have led to the development of several colorimetric chemical sensors capable of detecting MOX, CIP, and Cr(III) in diverse industrial applications [48–51]. Nevertheless, conventional detection

methods for MOX, CIP, and Cr(III) are typically performed separately. To date, the simultaneous detection of these three analytes using a single molecular platform has rarely been documented to the best of our knowledge. To address this limitation, we designed and synthesized a novel ammonium thioglycolate (ATG)-functionalized AuNP-based system and systematically evaluated its multi-analyte recognition capabilities. This system is anticipated to function as a versatile multi-analyte recognition sensor in metal ion detection, providing the simultaneous identification of multiple analytes within a single assay.

Herein, we proposed a novel platform comprising ammonium thioglycolate-functionalized AuNPs (ATG-AuNPs) that were employed as a colorimetric chemosensor based upon the aggregation of ATG-AuNPs upon binding to MOX, CIP, and Cr(III). This resulted in the color of the AuNPs changing from wine-red to blue-gray. The influencing factors were optimized to achieve the maximum sensitivity of the probe. Then, its analytical performances were assessed and confirmed before being used to detect MOX/CIP and Cr(III) in actual samples. Finally, the exploited sensing strategy will simultaneously sense multiple targets in realistic samples, paving the way for the potential application of AuNPs or other metal nanoparticles in the identification and differentiation of several targets, which has yet to be published.

## 2. Materials and Methods

### 2.1. Materials

Hydrogen tetrachloroaurate hydrate ( $\text{HAuCl}_4 \cdot 4\text{H}_2\text{O}$ ), ciprofloxacin ( $\text{C}_{17}\text{H}_{18}\text{FN}_3\text{O}_3$ ), trisodium citrate dihydrate ( $\text{C}_6\text{H}_5\text{Na}_3\text{O}_7 \cdot 3\text{H}_2\text{O}$ ), and ammonium thioglycolate ( $\text{C}_2\text{H}_7\text{NO}_2\text{S}$ ) were purchased from Aladdin Reagent Co., Ltd. (Shanghai, China). Moxifloxacin (MOX) hydrochloride ( $\text{C}_{21}\text{H}_{24}\text{FN}_3\text{O}_4$ ), tetracycline (TC), and other antibiotics were supplied by Shanghai Macklin Biochemical Co., Ltd. (Shanghai, China). Chromium chloride hexahydrate ( $\text{CrCl}_3 \cdot 6\text{H}_2\text{O}$ ) and other metal ions were purchased from Tianjin Guangfu Fine Chemical Institute (Tianjin, China). All aqueous solutions were prepared using ultra-pure water (18.2 M $\Omega$ , Miui-Q, Millipore) (Dubuque, IA, USA). All the reagents were of analytical grade unless otherwise indicated.

### 2.2. Apparatus

Transmission electron microscope (TEM) images were characterized using a JEM-1011 (Tokyo, Japan) operating at an accelerated voltage of 120 kV. Subsequently, the UV–visible absorbance spectra (UV–Vis) were measured on a Perkin Elmer Lambda 35 Spectrometer (Waltham, MA, USA) at room temperature in the 200–800 nm wavelength range.

### 2.3. Synthesis of AuNPs

According to the method reported by Frens [52], AuNPs with a 13 nm diameter were prepared by reducing  $\text{HAuCl}_4$  with citrate in an aqueous solution. All glassware utilized in the subsequent experimental process was pre-cleaned in a bath of freshly-generated  $\text{HNO}_3$ -HCl (1:3, *v/v*), washed successively with distilled water, and air-dried. Briefly, 1.0 mM AuNPs (100 mL) was injected into a 250 mL flask with a magnetic stirrer and heated to boiling. After that, 10 mL sodium citrate (38.8 mM) was quickly added into the above flask. Heating was stopped when a wine-red color was acquired, and then it was stirred at 125 °C for 30 min and allowed to cool to room temperature with successive stirring.

### 2.4. Modification of AuNPs by ATG

To modify the surface of the AuNPs by ATG, 160  $\mu\text{L}$  AuNPs solution was added into a mixed solvent of 4  $\mu\text{L}$  of ATG (4 mM) and 26  $\mu\text{L}$  double-deionized water, and the self-assembly reaction was performed at 400 rpm for 1 h at room temperature to produce ATG-AuNPs.

### 2.5. Colorimetric Detection

In brief, the ATG-AuNPs solution (164  $\mu\text{L}$ ) and 10  $\mu\text{L}$  of different MOX, CIP, and Cr(III) concentrations were blended and reacted for 1 min at room temperature with shaking. Then, the absorbance ratio of  $A_{600}/A_{520}$ ,  $A_{640}/A_{520}$ , and  $A_{650}/A_{520}$  was recorded by UV–Vis absorbance spectra. Furthermore, the specificity of the ATG-AuNPs was evaluated by testing with other antibiotics and ions, including Tetracycline (TC), Pefloxacin (PEF), Lomefloxacin Hydrochloride (LXN), Ampicillin trihydrate (AMP), Amoxicillin trihydrate (AMX), Oxytetracycline (OTC), Doxycycline hyclate (DOX), Gibberellic acid (GA), Azithromycin (AZM), Roxithromycin (ROX), Chloramphenicol (CM), Cr(III), Al(III), Mn(II), Pb(II), Cu(II), Hg(II), Ni(II), Fe(II), Ag(I), Fe(III), Zn(II), Ca(II), Ba(II), and Mg(II) (the concentration of all antibiotics and metals ions is 200  $\mu\text{M}$  and 10  $\mu\text{M}$ , respectively). The visual color changes were observed by the naked eye, and images of the samples were captured using a smartphone and subsequently recorded by UV–Vis spectra.

### 2.6. Detection of Real Samples

The applicability of ATG-AuNPs in actual environmental samples was evaluated. The tap water was taken from our laboratory, while the lake water was obtained from the Wenying Lake in Datong City, Shanxi Province. The real samples were pre-treated by centrifuging at 12,000 rpm for 10 min, and then filtered with a 0.22  $\mu\text{m}$  filter to eliminate insoluble matter. The ATG-AuNPs and the real water samples with three analytes were mixed and reacted for 1 min, and the color changes were recorded by UV–Vis absorbance spectra.

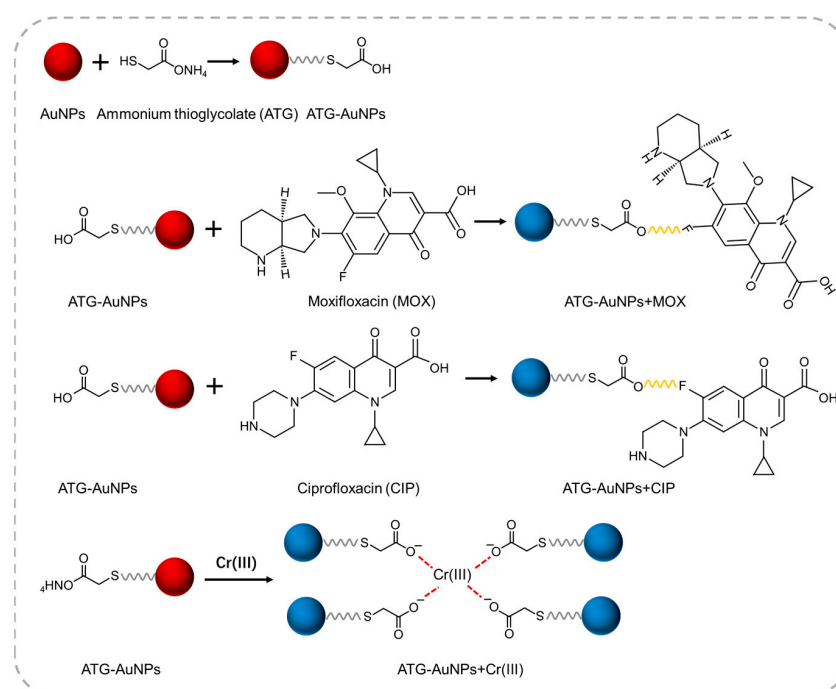
## 3. Results and Discussion

### 3.1. Preparation, Characterization, and Detection Mechanism of ATG-AuNPs

The possible detection mechanism of MOX/CIP and Cr(III) using ATG-AuNPs is shown in Scheme 1. The AuNPs employed in this study were synthesized via the well-established citrate-reducing approach, and then the AuNPs were modified and stabilized by the ATG ligands. This is likely because the Au-S bond was utilized to bind ATG on the surface of the AuNPs via a self-assembly reaction, similar to that previously reported in the paper [53]. After adding MOX and CIP containing fluorine in their chemical structure, the fluorine can interact with the carboxyl group of ATG selectively, induce aggregation of the ATG-AuNPs, and change the color from wine-red to blue-gray. In addition, in the presence of Cr(III), the carboxyl group of ATG can effectively capture and chelate Cr(III) ions, forming stable octahedral hexacoordinate complexes (excluding two solvent water molecules) [54–56]. This coordination interaction induces the aggregation of the ATG-AuNPs, along with a color change. As shown by transmission electron microscopy (TEM), the AuNPs and ATG-AuNPs displayed a nearly spherical shape, uniform particle size, and excellent dispersion. The average diameter of AuNPs is approximately 13 nm (Figure 1A(a,b)). Owing to their capacity to undergo interparticle surface plasmon coupling, the obtained diameter was appropriate for the colorimetric detection ( $>3.5$  nm), resulting in a noticeable color change from wine-red to blue-gray at the level of the nanomolar concentration. Once MOX/CIP and Cr(III) were added to a dispersion of the ATG-AuNPs nanoprobes, the rigid structure formed was insufficient to stabilize the AuNPs solution, leading to the aggregation of AuNPs (Figure 1A(c–e)).

The UV–Vis absorption spectrum was further employed to evaluate the surface plasmon resonance of the AuNPs before and after modification and the optical properties of the modified AuNPs. As illustrated in Figure 1B(a), AuNPs have a sharp absorption peak of 518 nm, a characteristic plasmon resonance absorption band. As expected, the absorption spectra of ATG-AuNPs were similar to those of AuNPs, and the color of the as-synthesized ATG-AuNPs solution still remained wine-red, suggesting that AuNPs do not aggregate

after modification (Figure 1B(b)). Significantly, the absorption peaks of ATG-AuNPs were red-shifted from 518 nm to 520 nm. These results concur with previous studies [57,58] indicating that the peak location of surface plasmon absorption is moderately red-shifted owing to changes in the refractive index around the AuNPs by surface functionalization. Upon adding MOX and CIP, the characteristic peak of the ATG-AuNPs at 520 nm diminished markedly, and a new peak at around 600 and 640 nm increased significantly, as illustrated in Figure 1B(c,d). Moreover, the presence of Cr(III) caused a notable decline in the characteristic peak of ATG-AuNPs at 520 nm, accompanied by an increase in a new peak at approximately 650 nm, as shown in Figure 1B(e). Meanwhile, the color changed from wine-red to blue-gray. The above results suggested that the modifier was successfully coated on the surface of the AuNPs to prepare the colorimetric sensors. In addition, the ATG-AuNPs have stable optical features (Figure S1), which is advantageous for analyzing MOX/CIP and Cr(III).



**Scheme 1.** Schematic illustration of a possible mechanism for the colorimetric chemosensing of MOX/CIP and Cr(III).

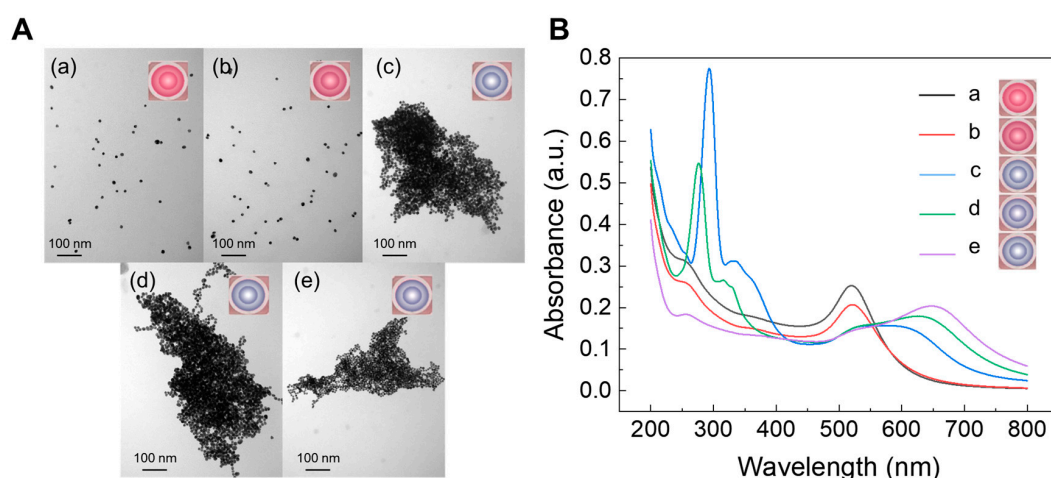


**Figure 1.** (A) TEM image and (B) UV-Vis absorption spectra of (a) AuNPs, (b) ATG-AuNPs, (c) ATG-AuNPs+MOX, (d) ATG-AuNPs+CIP, and (e) ATG-AuNPs+Cr(III).



### 3.2. Optimization of the Detection System

The parameters, including the modifier concentration and reaction time, were optimized to identify the optimal conditions for achieving enhanced responses from ATG-AuNPs as a colorimetric probe for identifying and determining MOX/CIP and Cr(III).

#### 3.2.1. The Effect of Concentration of ATG as a Modifier

As mentioned above, the concentration of the modifier is a crucial factor in colorimetric sensing devices, and it should be optimized. The optimal concentration of ATG should consider that not only is sufficient ATG needed to saturate the surface of AuNPs, but no free ATG is distributed in the solution. In this study, 160  $\mu\text{L}$  of AuNPs was mixed with various amounts of ATG to determine the concentration of ATG. As shown in Figure 2A, the absorption of AuNPs at 520 nm decreased significantly with increasing ATG concentrations up to 80  $\mu\text{M}$ , which could be ascribed to the existence of free ATG molecules. As anticipated, with the increasing ATG concentration, the absorption of ATG-AuNPs at 520 nm displayed a negligible change, indicating that almost the entire surface of the AuNPs was adsorbed completely by ATG molecules. This is likely because the -SH groups on the surface of the AuNPs have become saturated. Based on the above results, the optimal concentration value for ATG was 80  $\mu\text{M}$  and this was used for subsequent experiments.

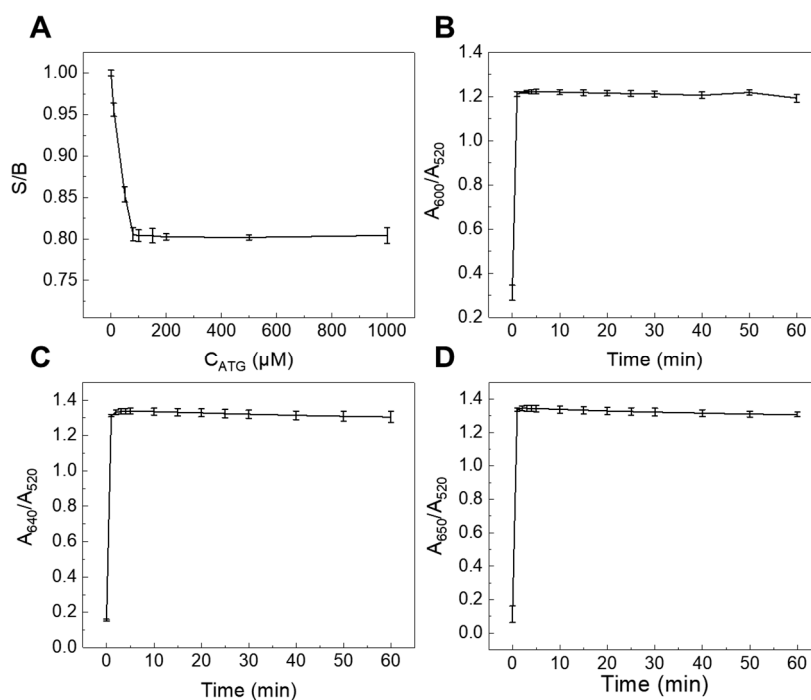


**Figure 2.** (A) The effect of concentrations of ATG (0~1000  $\mu\text{M}$ ) on the responsiveness of the AuNPs. The effect of reaction time on the responsiveness of the ATG-AuNPs sensor for MOX(200  $\mu\text{M}$ ) (B), CIP(100  $\mu\text{M}$ ) (C), and Cr(III) (10  $\mu\text{M}$ ) (D).

#### 3.2.2. The Effect of the Reaction Time

Response time is another critical metric for evaluating colorimetric chemosensors. The response time of ATG-AuNPs to MOX was determined by observing the change in color with reaction time. A color change was immediately observed when MOX was added to the ATG-AuNPs solution. The absorbance ratio versus the concentration of MOX (200  $\mu\text{M}$ ) showed an increasing sensitivity with the incubation time from 0 to 1 min (Figure 2B). However, it remained unchanged for longer periods (Figure S3). That means 1 min was adequate for the reaction of MOX and ATG. Additionally, the UV-Vis absorbance spectra of the reaction of CIP and Cr(III) with the ATG-AuNPs sensor were recorded for

60 min (Figures S4 and S5). The results revealed that the aggregation of ATG-AuNPs in the presence of CIP and Cr(III) was elevated up to 1 min and maintained unchanged (Figure 2C,D). Therefore, all the following tests for CIP and Cr(III) were performed with a responsive time of 1 min, respectively.

Furthermore, the aggregation of the ATG-AuNPs reduced the absorbance at a wavelength of 520 nm while increasing it at 600–650 nm. The sensitivity dependent on MOX reached a maximal value at  $A_{600}/A_{520}$  and remained unchanged at the larger wavelength (Figure S3). Therefore, the detection wavelengths were determined to be  $A_{600}/A_{520}$ . Additionally, the detection wavelengths for CIP and Cr(III) were fixed at  $A_{640}/A_{520}$  and  $A_{650}/A_{520}$ , respectively (Figures S4 and S5).

### 3.2.3. Selectivity Evaluation

To detect all types of water samples with complicated environments, a high-selectivity measurement assay is desired. To this end, 164  $\mu\text{L}$  ATG-AuNPs was mixed with 10  $\mu\text{L}$  MOX (200  $\mu\text{M}$ ) or different other antibiotics (200  $\mu\text{M}$ ) and metal ion (10  $\mu\text{M}$ ) solutions and incubated for 1 min. The investigated antibiotics and metal ions solutions include TC, CIP, PEF, LXN, AMP, AMX, OTC, DOX, GA, AZM, ROX, CM, Cr(III), Al(III), Mn(II), Pb(II), Cu(II), Hg(II), Ni(II), Fe(II), Ag(I), Fe(III), Zn(II), Ca(II), Ba(II), and Mg(II). As shown in Figure 3A,B, the addition of MOX, CIP, and Cr(III) to the ATG-AuNPs showed an apparent decrease at 520 nm and a new red-shifted peak at 600, 640, and 650 nm by UV–Vis absorbance spectra. Moreover, the presence of MOX/CIP and Cr(III) led to a color change of the ATG-AuNPs from wine-red to blue-gray. In contrast, other antibiotics and metal ions do not result in significant red-shift and color variations relative to the blank of ATG-AuNPs, which is ascribed to the high selectivity of ATG-AuNPs for MOX/CIP and Cr(III) due to the combining action of the carboxyl group of ATG on AuNPs.

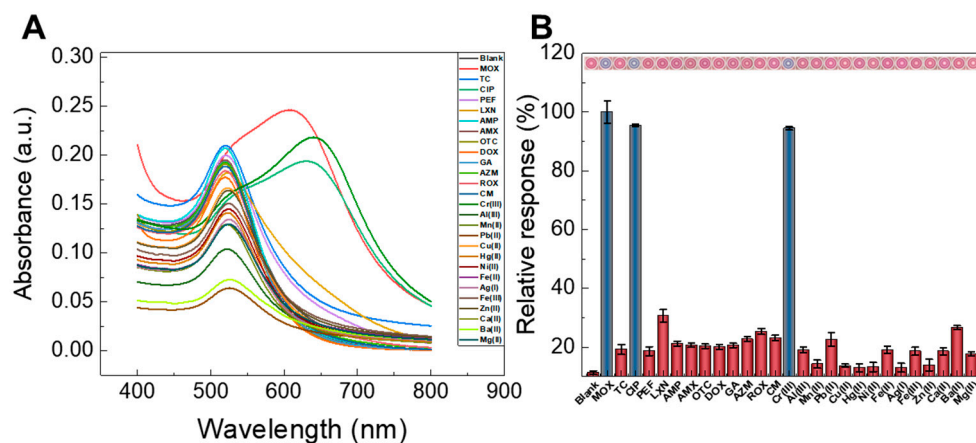


**Figure 3.** Selectiveness of the detection system. (A) UV–Vis absorption spectra and (B) the relative response of ATG-AuNPs towards MOX tested against some potential targets; inset: photos showing the corresponding sample color. MOX, TC, CIP, PEF, LXN, AMP, AMX, OTC, DOX, GA, AZM, ROX, and CM are 200  $\mu\text{M}$ , respectively, and Cr(III), Al(III), Mn(II), Pb(II), Cu(II), Hg(II), Ni(II), Fe(II), Ag(I), Fe(III), Zn(II), Ca(II), Ba(II), and Mg(II) are 10  $\mu\text{M}$ , respectively. (Blue-gray color: aggregation; wine-red color: dispersion).

### 3.2.4. Interference Study with Other Substances

To investigate the anti-interference ability of other substances on the performance of the ATG-AuNPs system for MOX/CIP and Cr(III), the determination and discrimination of three or two analytes were investigated in the presence of TC, PEF, LXN, AMP, AMX, OTC, DOX, GA, AZM, ROX, CM, Al(III), Mn(II), Pb(II), Cu(II), Hg(II), Ni(II), Fe(II), Ag(I), Fe(III), Zn(II), Ca(II), Ba(II), and Mg(II). Figure 4 illustrates the percentage response together with

the color change of the ATG-AuNPs sensor for various compounds in the addition of MOX (200  $\mu$ M)/CIP (200  $\mu$ M) and Cr(III) (10  $\mu$ M), MOX/Cr(III) (Figure S6), as well as MOX/CIP (Figure S7), as the aggregation of the nanoparticles is evident from the observed results and their color change occurred with the addition of different types target analytes, suggesting that the formation of chemical bonds between these analytes and ATG is much more robust than the other samples above. Therefore, the developed sensor is a valuable and reliable method for quantitatively measuring MOX/CIP and Cr(III) in actual samples.

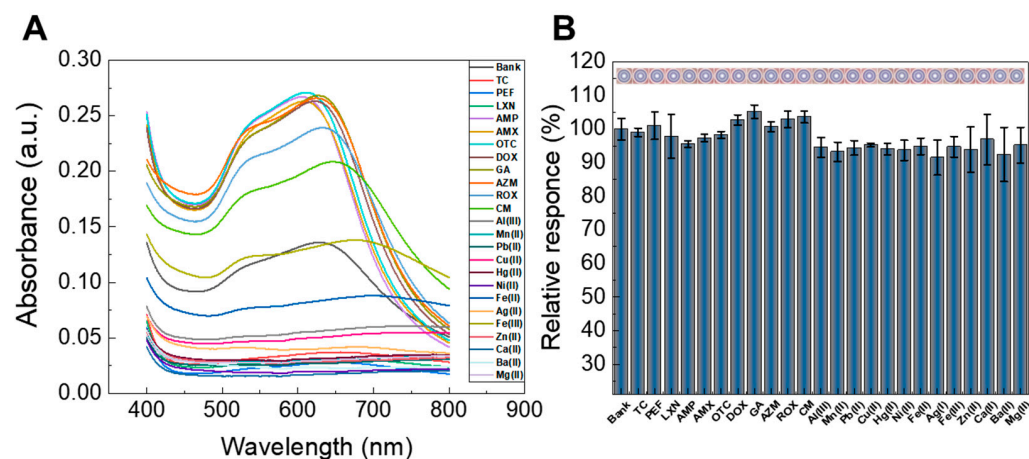


**Figure 4.** Anti-interference test for the detection system. (A) UV-Vis absorption spectra and (B) the relative response for the ATG-AuNPs system in the presence of MOX/CIP and Cr(III) and a mixture of MOX/CIP, Cr(III), and other potential targets; inset: photos showing the corresponding sample color. MOX, CIP, TC, PEF, LXN, AMP, AMX, OTC, DOX, GA, AZM, ROX, and CM are 200  $\mu$ M, respectively, and Cr(III), Al(III), Mn(II), Pb(II), Cu(II), Hg(II), Ni(II), Fe(II), Ag(I), Fe(III), Zn(II), Ca(II), Ba(II), and Mg(II) are 10  $\mu$ M, respectively.

### 3.2.5. Sensitive Detection

To investigate the sensitivity of the ATG-AuNPs assays for the quantitative detection of MOX/CIP and Cr(III), ATG-AuNPs were mixed with their solutions at different concentrations under optimized conditions. The photograph and UV-Vis absorbance spectra were collected. As the concentration of MOX increased from 0  $\mu$ M to 200  $\mu$ M, the color of the ATG-AuNPs gradually changed from wine-red to blue-gray (Figure 5A). The UV-Vis spectra of ATG-AuNPs showed that the characteristic absorbance peaks at 520 nm gradually declined along with increasing MOX concentration. In comparison, the red-shifted absorption band at 600 nm increased gradually. In addition, Figure 5B–D show the linear relationship ( $y = 0.0014x + 0.3203$ ,  $y = 0.0076x - 0.3083$ ) between the concentration of MOX ranging from 0 to 200  $\mu$ M and the logarithm of the  $A_{600}/A_{520}$  ratio, (with correlation coefficients of 0.9982 and 0.9971. The detection limit is 1.57  $\mu$ M by UV-Vis ( $S/\sigma = 3$ ), where  $S$  is the slope of the standard curve, and  $\sigma$  is the calibration deviation of the blank.

Furthermore, with a gradually increasing CIP concentration (0–100  $\mu$ M) in the ATG-AuNPs solution, the characteristic absorption peak at 520 nm was red-shifted to 640 nm. Meanwhile, a gradual decrease was found in the absorption spectra at 520 nm. In addition, the intensity of the absorption peak of the ATG-AuNPs at 650 nm was notably improved with the gradually increasing Cr(III) concentration (0–10  $\mu$ M). The corresponding absorbance calibration curve was plotted versus CIP or Cr(III) concentration (Figures 6 and 7). Satisfactory linear relationships were obtained for CIP and Cr(III), with  $R^2 = 0.9925$  and 0.9993 correlation coefficients, respectively. The detection limit (LOD) of the ATG-AuNPs for CIP and Cr(III) is computed to be 1.30  $\mu$ M and 57.1 nM, respectively.



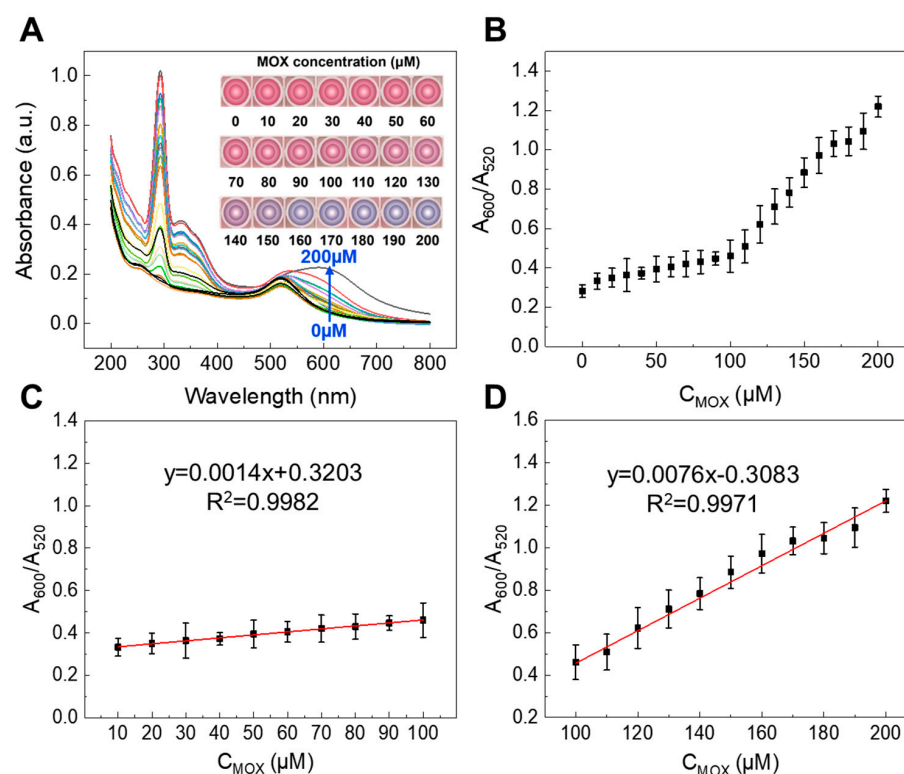


**Figure 5.** The detection of MOX using the ATG-AuNPs. (A) The change in the UV–Vis absorption spectra was recorded for the ATG-modified AuNPs upon increasing the MOX concentration; inset: photos showing the corresponding sample color. (B) The relationship between  $A_{600\text{nm}}/A_{520\text{nm}}$  and the MOX concentration. The linear calibration curve with different concentrations: (C) MOX (0~100  $\mu\text{M}$ ) and (D) MOX (100~200  $\mu\text{M}$ ).

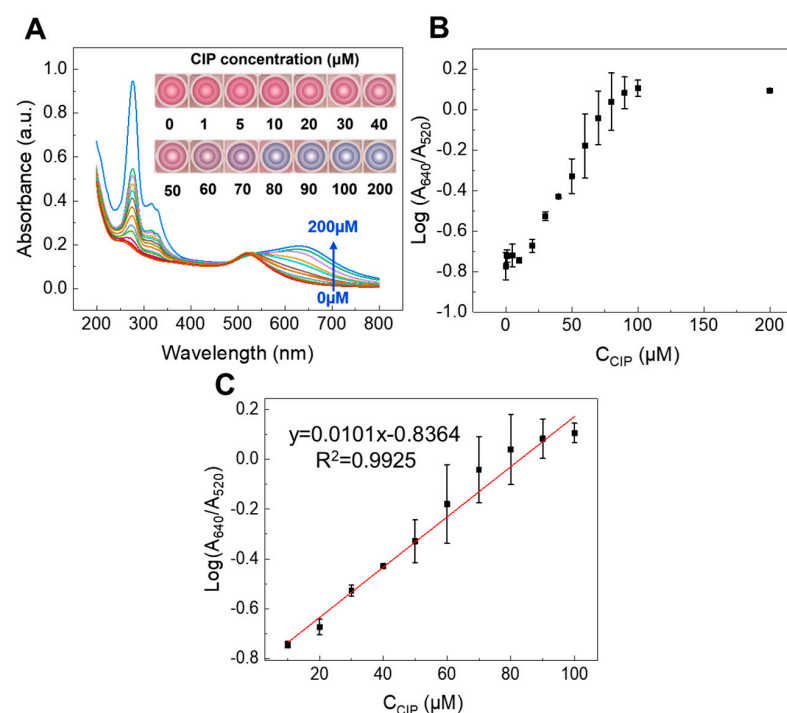


**Figure 6.** The detection of CIP using the ATG-AuNPs. (A) The change in the UV–Vis absorption spectra was recorded for the ATG-modified AuNPs upon increasing the CIP concentration; inset: photos showing the corresponding sample color. (B) The relationship between  $\text{Log}(A_{640\text{nm}}/A_{520\text{nm}})$  and the CIP concentration. (C) The linear calibration curve with different concentrations CIP (0~100  $\mu\text{M}$ ).

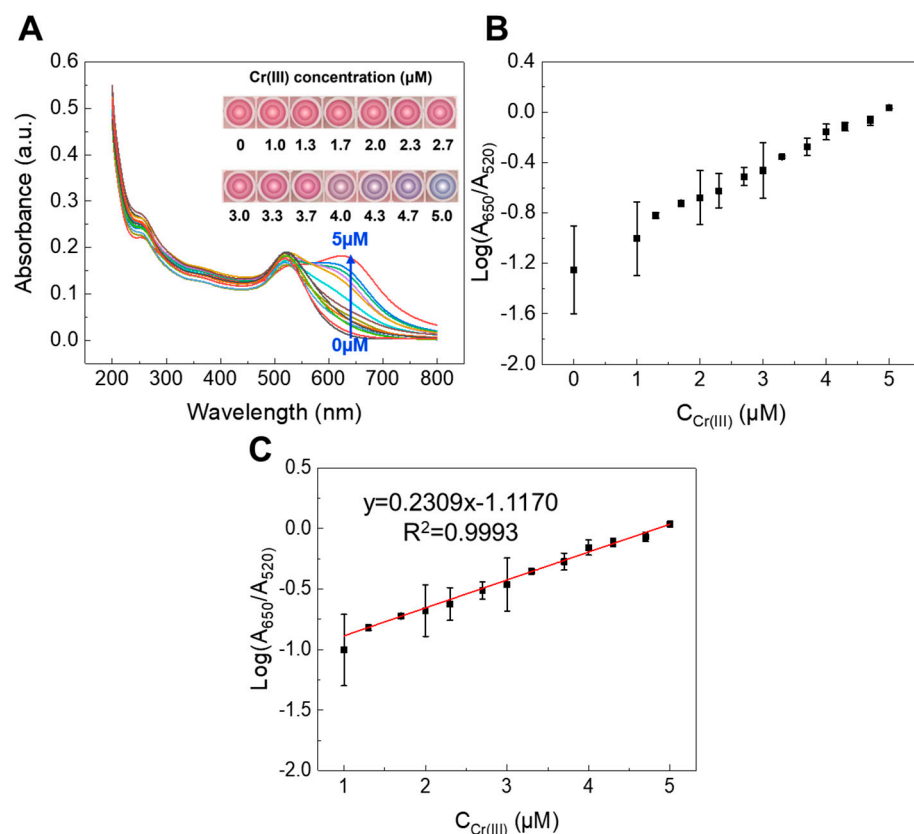


**Figure 7.** The detection of Cr(III) using the ATG-AuNPs. **(A)** The change in the UV–Vis absorption spectra was recorded for the ATG-modified AuNPs upon increasing the CIP concentration; inset: photos showing the corresponding sample color. **(B)** The relationship between  $\text{Log}(A_{650\text{nm}}/A_{520\text{nm}})$  and the Cr(III) concentration. **(C)** The linear calibration curve with different concentrations Cr(III) (0~5.0  $\mu\text{M}$ ).

Table S1 compares the current methods with previous methods for quantitatively detecting MOX/CIP and Cr(III). It shows that the LOD and dynamic range of the proposed ATG-AuNPs nanosensor are enhanced compared with other reported methods. Thus, based on the above results, the developed method has a comparative or even better performance and can be considered a novel standalone system that can meet the demand for the simple, fast, and sensitive simultaneous detection of MOX/CIP and Cr(III).

### 3.2.6. Investigation of the Performance of ATG-AuNPs Sensor in Actual Samples

The colorimetric detection capability of ATG-AuNPs in the actual environment was investigated by spiked recovery experiments on complex samples. Two standard practical samples were chosen: tap water and lake water (Table 1). The standard additive approach has been applied to avoid the effects of the matrix. In this way, several analyte concentrations within the calibration curve range were added to the probe with actual samples under optimal conditions. The analysis method was carried out in the same manner as described in the Section 2, and then the results were reported. According to the obtained results, the recoveries obtained were in the range of 96.42~98.77%, 96.85~99.71%, and 97.00~99.54% for MOX, CIP, and Cr(III), respectively, which demonstrated that the ATG-AuNPs probe as an inexpensive and straightforward colorimetric sensor has an outstanding efficiency and performance for the simultaneous detection of MOX/CIP and Cr(III) in actual samples.

**Table 1.** Practical application of developed sensor with tap and lake water.

Samples		Added ( $\mu\text{M}$ )	Tap Water			Lake Water		
			Measured ( $\mu\text{M}$ )	Recovery (%)	RSD (%)	Measured ( $\mu\text{M}$ )	Recovery (%)	RSD (%)
MOX	1	20	19.29	97.87	3.40	19.35	96.77	3.40
	2	30	28.92	96.42	3.53	29.59	98.77	3.34
	3	40	38.95	97.38	3.07	38.93	97.33	2.20
CIP	1	20	19.61	98.05	0.46	19.37	96.85	1.96
	2	30	29.84	99.46	2.50	29.89	99.62	3.30
	3	40	39.85	99.63	1.30	39.88	99.71	2.70
Cr(III)	1	1	1.00	99.54	2.37	0.99	99.08	0.93
	2	2	1.95	97.70	2.70	1.94	97.00	0.40
	3	3	2.98	99.50	1.60	2.93	97.62	1.10

Finally, to evaluate the accuracy and precision of the proposed method, repeatability tests were conducted. Intra-day ( $n = 10$ ) repeatability tests demonstrated the RSD values for MOX, CIP, and Cr(III) were lower than 1.4%, 1.4%, and 4.1%, respectively (Figures S7, S8, and S9). These values indicate that the developed method exhibits excellent accuracy and precision.

#### 4. Conclusions

In conclusion, ATG-AuNPs as a colorimetric sensor were prepared using a simple, low-cost, and extensible strategy through the chemical synthesis of AuNPs and subsequently by surface modification with ATG. Transmission electron microscopy (TEM) verified the successful preparation and modification of AuNPs and ATG-AuNPs. Interestingly, after modification by ATG, low levels of three analytes were investigated by the ATG-AuNPs probe, and the sensor's aggregation and color change were found. Investigating various parameters indicated that the maximum response of the ATG-AuNPs sensor for detecting MOX/CIP and Cr(III) was obtained in 80  $\mu\text{M}$  and 1 min. The results confirmed that the ATG-AuNPs sensor's sensitivity was high, and its detection limit was observed at 1.57  $\mu\text{M}$ , 1.03  $\mu\text{M}$ , and 57.1 nM for MOX, CIP, and Cr(III), respectively. The recovery by utilizing this sensor in an actual sample was observed to be in the range of 96.42~98.77%, 96.85~99.71%, and 97.00~99.54% for MOX/CIP and Cr(III), which demonstrated that the ATG-AuNPs probe as a simple, rapid, and inexpensive colorimetric sensor has an outstanding performance and efficiency for simultaneously determining MOX/CIP and Cr(III) in actual samples.

**Supplementary Materials:** The following supporting information can be downloaded at <https://www.mdpi.com/article/10.3390/s25103228/s1>, Electronic Supplementary Information (ESI) available: Experimental figures.

**Author Contributions:** L.Z., J.S. and J.L. conceived the idea of the work; L.Z. performed the research, analyzed data, and wrote the paper. J.W. carried out research investigation and data curation. X.Y. and F.F. contributed to refining ideas, additional analyses, and finalizing this paper. All authors have read and agreed to the published version of the manuscript.

**Funding:** This work was supported by the National Natural Science Foundation of China (No. 22476118), the Fundamental Research Program of Datong City (No. 2023058), and the Innovation and Entrepreneurship Training Program for College Students in Shanxi Province (No. XDC2023121).

**Institutional Review Board Statement:** Not applicable.

**Informed Consent Statement:** Not applicable.

**Data Availability Statement:** The datasets used and/or analyzed during the current study are available from the corresponding author upon reasonable request.

**Acknowledgments:** We sincerely thank Yani Wang from the Shanxi Inspection and Testing Center for her significant contributions made during the process of drafting, reviewing, and editing this manuscript.

**Conflicts of Interest:** The authors declare no competing financial interests.

## References

1. Zhou, Q.; Long, N.; Liu, L.; Zhai, H.Y.; Zhu, M.F. Electrochemical determination of moxifloxacin hydrochloride based on molecularly imprinted polymer modified carbon paste electrode. *Int. J. Electrochem. Sci.* **2015**, *10*, 5069–5076. [\[CrossRef\]](#)
2. Zhan, X.Y.; Zhang, Z.L.; Lin, J.; Xu, J.C.; Wang, Q.X.; Hong, B.; Xia, Y.C.; Zeng, Y.X. Surface atom rearrangement enabling graphitic carbon nitride/sodium alginate gel monolith for ultrafast completely photodegrading ciprofloxacin under visible light. *Chem. Eng. J.* **2024**, *489*, 151218. [\[CrossRef\]](#)
3. Singha, S.; Ahn, K.H. Detection of ciprofloxacin in urine through sensitized anthanide luminescence. *Sensors* **2016**, *16*, 2065. [\[CrossRef\]](#)
4. Sajwan, R.K.; Shailja, P.; Kumar, R.; Dhiman, T.K.; Eremin, S.A.; Solanki, P.R. Enhanced fluorescence of mercaptopropionic acid-capped zinc sulfide quantum dots with moxifloxacin in food and water samples via reductive photoinduced electron transfer. *Environ. Sci. Nano* **2021**, *8*, 2693–2705. [\[CrossRef\]](#)
5. Mohaghegh, F.; Tehrani, A.M.; Rana, D.; Winterhalter, M.; Materny, A. Detection and quantification of small concentrations of moxifloxacin using surface-enhanced Raman spectroscopy in a Kretschmann configuration. *J. Raman Spectrosc.* **2021**, *52*, 1617–1629. [\[CrossRef\]](#)
6. Wang, Y.; Xu, D.; Yang, X.; He, J.-H. Novel 2D/2D S-scheme heterojunction photocatalyst for peroxydisulfate activation enables ciprofloxacin ultrafast degradation: High-efficiency photogenerated carrier transport. *Chem. Eng. J.* **2024**, *488*, 150844. [\[CrossRef\]](#)
7. European Economic Community. *EEC Commission Regulation (EEC) No. 2901/93 of 23/10/93*; European Economic Community: Brussels, Belgium, 1993.
8. Zhang, L.X.; Tang, S.Y.; He, F.X.; Liu, Y.; Mao, W.; Guan, Y.T. Highly efficient and selective capture of heavy metals by poly(acrylic acid) grafted chitosan and biochar composite for wastewater treatment. *Chem. Eng. J.* **2019**, *378*, 122215. [\[CrossRef\]](#)
9. Zheng, P.; Li, M.; Jurevic, R.; Cushing, S.K.; Liu, Y.X.; Wu, N.Q. A gold nanohole array based surface-enhanced Raman scattering biosensor for detection of silver(I) and mercury(II) in human saliva. *Nanoscale* **2015**, *7*, 11005–11012. [\[CrossRef\]](#)
10. Jahrman, E.P.; Seidler, G.T.; Sieber, J.R. Determination of hexavalent chromium fractions in plastics using laboratory-based, high-resolution X-ray emission spectroscopy. *Anal. Chem.* **2018**, *90*, 6587–6593. [\[CrossRef\]](#)
11. Eastmond, D.A.; Macgregor, J.T.; Slesinski, R.S. Trivalent chromium: Assessing the genotoxic risk of an essential trace element and widely used human and animal nutritional supplement. *Crit. Rev. Toxicol.* **2008**, *38*, 173–190. [\[CrossRef\]](#)
12. Abdelaziz, A.A.; Elbanna, T.E.; Gamaleldeen, N.M. Validated microbiological and HPLC methods for the determination of moxifloxacin in pharmaceutical preparations and human plasma. *Braz. J. Microbiol.* **2012**, *43*, 1291–1301. [\[CrossRef\]](#) [\[PubMed\]](#)
13. Scherer, R.; Pereira, J.; Firme, J.; Lemos, M.; Lemos, M. Determination of Ciprofloxacin in Pharmaceutical Formulations Using HPLC Method with UV Detection. *Indian J. Pharm. Sci.* **2014**, *76*, 541–544. [\[PubMed\]](#)
14. Ahmed, R.M.; Hadad, G.M.; El-Gendy, A.E.; Ibrahim, A. Development of HPLC method for determination of sitagliptin in human plasma using fluorescence detector by experimental design approach. *Anal. Chem. Lett.* **2018**, *8*, 813–828. [\[CrossRef\]](#)
15. Zhao, X.X.; Yuan, Y.J.; Shao, Q.; Qiao, H.Q. Simultaneous determination of moxifloxacin hydrochloride and dexamethasone sodium phosphate in rabbit ocular tissues and plasma by LC-MS/MS: Application for pharmacokinetics studies. *Molecules* **2022**, *27*, 7934. [\[CrossRef\]](#)
16. Ramadan, L.; Ozturk-Ufuk, I.; Yuksel, E.; Topuz, E. Development of LC-MS/MS Method for the Simultaneous Detection of Emerging Contaminants in Aquatic Matrices. *Water Air Soil Pollut.* **2024**, *235*, 537. [\[CrossRef\]](#)
17. Raju, B.; Ramesh, M.; Borkar, R.M.; Padiya, R.; Banerjee, S.K.; Srinivas, R. Development and validation of liquid chromatography-mass spectrometric method for simultaneous determination of moxifloxacin and ketorolac in rat plasma: Application to pharmacokinetic study. *Biomed. Chromatogr.* **2012**, *26*, 1341–1347. [\[CrossRef\]](#)
18. Loh, G.O.K.; Wong, E.Y.L.; Tan, Y.T.F.; Lee, Y.L.; Pang, L.H.; Chin, M.C.; Damenthi, N.; Peh, K.K. Simple and rapid LC-MS/MS method for determination of sitagliptin in human plasma and application to bioequivalence study. *J. Chromatogr. B* **2020**, *1159*, 122337. [\[CrossRef\]](#)

19. Kuznetsova, O.V.; Timerbaev, A.R. Direct seawater analysis by high-resolution ICP-MS provides insights into toxic metal accumulation in marine sediments. *Atomic Spectrosc.* **2021**, *42*, 85–90. [[CrossRef](#)]
20. Aydin, F.A.; Soylak, M. Separation, preconcentration and inductively coupled plasma-mass spectrometric (ICP-MS) determination of thorium(IV), titanium(IV), iron(III), lead(II) and chromium(III) on 2-nitroso-1-naphthol impregnated MCI GEL CHP20P resin. *J. Hazard. Mater.* **2010**, *173*, 669–674. [[CrossRef](#)]
21. Zhang, Y.L.; Zhang, Y.; Jarmal, R.; Abdirym, T. Highly Sensitive electrochemical sensing of moxifloxacin based on molecularly imprinted and Au nanoparticle functionalized PEDOT composites. *Chem. Eng. J.* **2024**, *498*, 155314. [[CrossRef](#)]
22. Liu, R.; Zhang, C.J.; Wu, T.H.; Liu, R.J.; Sun, J.; Ma, J. Fabrication of a novel HKUST-1/CoFe<sub>2</sub>O<sub>4</sub>/g-C<sub>3</sub>N<sub>4</sub> electrode for the electrochemical detection of ciprofloxacin in physiological samples. *Talanta* **2024**, *273*, 125882. [[CrossRef](#)]
23. Panagopoulou, C.; Skotadis, E.; Aslanidis, E.; Tzourmana, G.; Rapesi, A.; Tsioustas, C.; Kainourgiaki, M.; Kleitsiotis, G.; Tsekenis, G.; Tsoukalas, D. Non-Faradaic Impedimetric Detection of Heavy Metal Ions via a Hybrid Nanoparticle-DNAzyme Biosensor. *Biosensors* **2024**, *14*, 321. [[CrossRef](#)] [[PubMed](#)]
24. Al-Ghannam, S.M. Atomic absorption spectroscopic, conductometric and colorimetric methods for determination of some fluoroquinolone antibacterials using ammonium reineckate. *Spectrochim. Acta Part A Mol. Biomol. Spectrosc.* **2008**, *69*, 1188–1194. [[CrossRef](#)]
25. Altunay, N.; Yildirim, E.; Gurkan, R. Extraction and preconcentration of trace Al and Cr from vegetable samples by vortex-assisted ionic liquid-based dispersive liquid–liquid microextraction prior to atomic absorption spectrometric determination. *Food Chem.* **2018**, *245*, 586–594. [[CrossRef](#)] [[PubMed](#)]
26. Sajwan, R.K.; Himanshu, J.K.; Solanki, P.R. Polyvinyl alcohol-derived-carbon quantum dots based fluorometric “On-Off” probe for moxifloxacin detection in milk and egg samples. *Food Chem.* **2024**, *439*, 138038. [[CrossRef](#)]
27. Li, Y.; Li, Q.; Wu, X.; Li, Z.; Mao, S. Dual-lanthanide cyclodextrin-polyoxometalate fluorescent assembly for rapid and sensitive detection of ciprofloxacin. *Sens. Actuat. B Chem.* **2024**, *418*, 136297. [[CrossRef](#)]
28. Chen, J.; Yin, C.; Zhao, B.; Cheng, X.Y. Strategies for preparation of chitosan based water-soluble fluorescent probes to detect Cr<sup>3+</sup> and Cu<sup>2+</sup> ions. *Int. J. Biol. Macromol.* **2024**, *276*, 133915. [[CrossRef](#)] [[PubMed](#)]
29. Jin, Z.C.; Yin, W.J.; Retout, M.; Housel, E.; Zhong, W.B.; Zhou, J.J.; Strano, M.S.; Jokerst, J.V. Colorimetric sensing for translational applications: From colorants to mechanisms. *Chem. Soc. Rev.* **2024**, *15*, 7681–7741. [[CrossRef](#)]
30. Elghanian, R.; Storhoff, J.J.; Mucic, R.C.; Letsinger, R.L.; Mirkin, C.A. Selective colorimetric detection of polynucleotides based on the distance-dependent optical properties of gold nanoparticles. *Science* **1997**, *277*, 1078–1081. [[CrossRef](#)]
31. Yue, G.Z.; Su, S.; Li, N.; Shuai, M.; Lai, X.C.; Astruc, D.; Zhao, P.X. Gold nanoparticles as sensors in the colorimetric and fluorescence detection of chemical warfare agents. *Coord. Chem. Rev.* **2016**, *311*, 75–84. [[CrossRef](#)]
32. Chen, H.; Cai, S.T.; Luo, J.X.; Liu, X.H.; Ou, L.J.; Zhang, Q.W.; Liedberg, B.; Wang, Y. Colorimetric biosensing assays based on gold nanoparticles functionalized/combined with non-antibody recognition elements. *TrAC Trends Anal. Chem.* **2024**, *173*, 117654. [[CrossRef](#)]
33. Zhai, R.Q.; Chen, G.; Liu, G.Y.; Huang, X.D.; Xu, X.M.; Li, L.Y.; Zhang, Y.G.; Wang, J.; Jin, M.J.; Xu, D.H.; et al. Enzyme inhibition methods based on Au nanomaterials for rapid detection of organophosphorus pesticides in agricultural and environmental samples: A review. *J. Adv. Res.* **2021**, *28*, 61–74. [[CrossRef](#)] [[PubMed](#)]
34. Yu, L.L.; Song, Z.R.; Peng, J.; Yang, M.L.; Zhi, H.; He, H. Progress of gold nanomaterials for colorimetric sensing based on different strategies. *TrAC Trends Anal. Chem.* **2020**, *127*, 115880. [[CrossRef](#)]
35. Liu, D.M.; Dong, C. Gold nanoparticles as colorimetric probes in food analysis: Progress and challenges. *Food Chem.* **2023**, *429*, 136887. [[CrossRef](#)] [[PubMed](#)]
36. Cheng, C.; Qiao, J.; Zhang, H.Y.; Zhao, Z.W.; Qi, L. Polymer-capped gold nanoparticles as nanozymes with improved catalytic activity for the monitoring of serum ciprofloxacin. *Analyst* **2022**, *147*, 1509–1514. [[CrossRef](#)]
37. Zehra, T.; Ahsan, F.; Versiani, M.A.; Wahid, S.; Jahangir, S.; Shah, M.R. Puerarin-coated gold nanoparticles (PUE-AuNPs) synthesized via green synthetic route: A new colorimetric probe for the detection of ciprofloxacin. *Turk. J. Chem.* **2021**, *45*, 1814–1827. [[PubMed](#)]
38. Trivedi, M.U.; Sharma, P.; Kaur, A.; Sharma, R.K. Unraveling the β-Cyclodextrin-Driven Inclusion Complexation with Phenylalanine-Capped AuNPs for Colorimetric Detection of Cr(III) and Fe(III). *ACS Appl. Nano Mater.* **2024**, *7*, 4377–4387. [[CrossRef](#)]
39. Zhang, Z.K.; Dong, Q.; Cao, Y.P.; Liu, Y.M.; Zhao, Y. Colorimetric Detection of Chromium Ions in Aqueous Solution Based on Functionalized Gold Nanoparticles with 4-Mercaptobenzoic Acid and Polyethyleneimine. *Nano* **2022**, *17*, 2250105. [[CrossRef](#)]
40. Liu, J.F.; Wang, X.K.; Zhu, X.F.; Zhao, Y.F.; Ye, Y. Advances in dual-function bioprobes for simultaneous detection of transition metal ions (Fe, Cu, Zn) and bioactive species. *Coord. Chem. Rev.* **2025**, *526*, 216352. [[CrossRef](#)]
41. Zhu, J.P.; Graziotto, M.E.; Cottam, V.; Hawtrey, T.; Adair, L.D.; Trist, B.G.; Pham, N.T.H.; Rouaen, J.R.C.; Ohno, C.; Heisler, M.; et al. Near-Infrared Ratiometric Fluorescent Probe for Detecting Endogenous Cu<sup>2+</sup> in the Brain. *ACS Sens.* **2024**, *9*, 2858–2868. [[CrossRef](#)]



42. Zhang, H.T.; Feng, L.; Jiang, Y.; Wong, Y.T.; He, Y.H.; Zheng, G.S.; He, J.; Tan, Y.; Sun, H.Y.; Ho, D. A reaction-based near-infrared fluorescent sensor for Cu<sup>2+</sup> detection in aqueous buffer and its application in living cells and tissues imaging. *Biosens. Bioelectron.* **2017**, *94*, 24–29. [\[CrossRef\]](#)
43. Zhang, L.M.; Han, Y.Y.; Zhao, F.; Shi, G.Y.; Tian, Y. A Selective and Accurate Ratiometric Electrochemical Biosensor for Monitoring of Cu<sup>2+</sup> Ions in a Rat Brain. *Anal. Chem.* **2015**, *87*, 2931–2936. [\[CrossRef\]](#)
44. Chen, S.Y.; Li, Z.; Li, K.; Yu, X.Q. Small molecular fluorescent probes for the detection of lead, cadmium and mercury ions. *Coord. Chem. Rev.* **2021**, *429*, 213691. [\[CrossRef\]](#)
45. Shi, J.Y.; Wu, S.Y.; Xue, Y.; Xie, Q.; Danzeng, Q.Z.; Liu, C.; Zhou, C.H. Fluorescence/colorimetric dual-signal sensor based on carbon dots and gold nanoparticles for visual quantification of Cr<sup>3+</sup>. *Microchim. Acta* **2024**, *191*, 571. [\[CrossRef\]](#)
46. Mahmoudi, H.; Bahram, M.; Dadashi, R. Colorimetric detection of sitagliptin and moxifloxacin using AgNPs modified by 4-mercaptophenylboronic acid. *Inorg. Chem. Commun.* **2024**, *167*, 112834. [\[CrossRef\]](#)
47. Shellaiah, M.; Simon, T.; Venkatesan, P.; Sun, K.W.; Ko, F.H.; Wu, S.P. Nanodiamonds conjugated to gold nanoparticles for colorimetric detection of clenbuterol and chromium(III) in urine. *Microchim. Acta* **2017**, *185*, 74. [\[CrossRef\]](#)
48. Li, S.; Wei, T.; Ren, G.; Chai, F.; Wu, H.; Qu, F. Gold nanoparticles based colorimetric probe for Cr(III) and Cr(VI) detection. *Colloids Surf. A Physicochem. Eng. Asp.* **2017**, *535*, 215–224. [\[CrossRef\]](#)
49. Karn-Orachai, K.; Wattanasin, P.; Ngamaroonchote, A. Colorimetric Sensor for Cr(VI) Ion Detection in Tap Water Using a Combination of AuNPs and AgNPs. *ACS Omega* **2024**, *9*, 26472–26483. [\[CrossRef\]](#)
50. Huang, W.W.; Wang, Y.C.; Wang, L.M.; Pan, C.Q.; Shen, G.Q. Colorimetric detection of ciprofloxacin in aqueous solution based on an unmodified aptamer and the aggregation of gold nanoparticles. *Anal. Methods* **2021**, *13*, 90–98. [\[CrossRef\]](#)
51. Nawaz, A.; Ali, S.M.; Rana, N.F.; Tanweer, T.; Batool, A.; Webster, T.J.; Mena, F.; Riaz, S.; Rehman, Z.; Batool, F.; et al. Ciprofloxacin-Loaded Gold Nanoparticles against Antimicrobial Resistance: An In Vivo Assessment. *Nanomaterials* **2021**, *11*, 3152. [\[CrossRef\]](#)
52. Frens, G. Controlled nucleation for the regulation of the particle size in monodisperse gold suspensions. *Nat. Phys. Sci.* **1973**, *241*, 20–22. [\[CrossRef\]](#)
53. Zhou, Y.; Zhao, H.; He, Y.J.; Ding, N.; Cao, Q. Colorimetric detection of Cu<sup>2+</sup> using 4-mercaptobenzoic acid modified silver nanoparticles. *Colloids Surf. A Physicochem. Eng. Asp.* **2011**, *391*, 179–183. [\[CrossRef\]](#)
54. Hemmateenejad, B.; Safavi, A.; Honarasa, F. Determination of nanoparticles concentration by multivariate curve resolution. *Chemom. Intell. Lab. Syst.* **2015**, *141*, 88–93. [\[CrossRef\]](#)
55. Lin, W.; Zhou, Y.S.; Zhao, Y.; Zhu, Q.S.; Wu, Y. Cr<sup>3+</sup>/COO<sup>−</sup> complexation induced aggregation of gelatin in dilute solution. *Macromolecules* **2002**, *35*, 7407–7413. [\[CrossRef\]](#)
56. Shadab, F.; Gholamreza, K.; Hamed, G.; Raouf, G. A paper-based optical probe for chromium by using gold nanoparticles modified with 2,2'-thiodiacetic acid and smartphone camera readout. *Microchim. Acta* **2018**, *185*, 374.
57. Heo, D.N.; Yang, D.H.; Moon, H.-J.; Lee, J.B.; Bae, M.S.; Lee, S.C.; Lee, W.J.; Sun, I.-C.; Kwon, I.K. Gold nanoparticles surface-functionalized with paclitaxel drug and biotin receptor as theranostic agents for cancer therapy. *Biomaterials* **2012**, *33*, 856–866. [\[CrossRef\]](#)
58. Yılmaz, D.D.; Demirezen, D.A.; Mihçioğur, H. Colorimetric detection of mercury ion using chlorophyll functionalized green silver nanoparticles in aqueous medium. *Surfaces Interfaces* **2021**, *22*, 100840. [\[CrossRef\]](#)

**Disclaimer/Publisher's Note:** The statements, opinions and data contained in all publications are solely those of the individual author(s) and contributor(s) and not of MDPI and/or the editor(s). MDPI and/or the editor(s) disclaim responsibility for any injury to people or property resulting from any ideas, methods, instructions or products referred to in the content.